A novel electrochemiluminescence biosensing system using photonic crystal as luminescence enhanced substrates for the ultrasensitive detection of food-borne harmful substances

Harrison Hao-Tian Tang[*, a], Hai-Jie Lu[b]
[a]Shanghai High School International Division (SHSID), Shanghai, China; [b]Institute of Advanced Materials and Flexible Electronics (IAMFE), School of Chemistry and Materials Science, Nanjing University of Information Science & Technology, Nanjing, China, 58731101, 2luhaijie@126.com

ABSTRACT

Safeguarding food quality and safety is essential to people's livelihoods. Over recent years, the ingestion of food-borne pathogens and their related metabolic toxins increasingly affects public health, leading to food poisoning reactions such as diarrhea or fever and even severe risks of cancer. To ensure food safety and public health, it is urgent to develop a novel, highly sensitive detection method for tracing harmful food-borne substances to accurately and quickly identify food-borne pathogens and their metabolic toxins that exceed regulatory standards. In this novel food-borne harmful substance detection approach, TiO_2 photonic crystal is used as the enhanced substrate. Through light scattering and plasmon resonance effects, the ECL signal strength of CdS quantum dots is greatly increased, and the detection sensitivity of the ECL sensor is improved, which provides a new idea for the design of POCT-ECL biosensors based upon enhanced substrates. This biosensor can accurately identify typical food-borne pathogenic bacteria such as Salmonella, metabolic toxins such as Aflatoxin, and heavy metal ions such as mercury, providing a powerful tool for ensuring food safety.

Keywords: Electrochemiluminescence, Point-Of-Care Technology, Photonic Crystals, Biosensor Prototype, Food Safety

1. INTRODUCTION

In the past few decades, food safety issue, or the health-affecting concerns of toxic or harmful food substances, has always been a severe threat to human health [1]. A closed mouth catches no flies, but food-borne harmful substances such as Aflatoxin, Salmonella, and Mercury (Hg^{2+}) ions inevitably still exist after decades of regulation [2]. Among these toxins, aflatoxin as WHO Group 1 Carcinogens [3] exist commonly in present food sources but are not visible under human eyes and cultivates during farming, harvest, and even post-harvest processes [4]. Aflatoxin B1 causes severe harm to human health, such as impaired growth, nausea, and even hepatocellular carcinoma [5]. To ensure public food safety, researchers have developed various methods for Aflatoxin detection over the past century [6]. Traditional methods of aflatoxin B1 detection include thin layer chromatography and liquid chromatography involving mixture separation for component analysis [7-8] where the steps of dissolving, solvent transferring, and mixture breakdown need long detection periods.

Nowadays, pathogenic bacteria of couple micrometers exist commonly in present food sources but are not visible under human eyes, with many common types [9]. These pathogenic bacteria have various effects on humans, such as emesia, fever, severe dehydration, and even death. In order to ensure food safety for the public, small-sized pathogenic bacteria detection has become extremely important, and researchers have devised various methods of examining them over the past century. To detect Salmonella using traditional methods, researchers put the target substance into an SS Agar chromogenic medium, where chromogenesis can lead to the formation of stained bacterial colonies to indicate the presence of the bacteria [10]. In this process, the steps of bacteria enrichment, buffered peptone water usage, chromogenesis, and biological experiments are relatively inefficient and have a higher false-positive rate [11].

Mercury ions in food can cause severe effects, such as permanent neurological damage and Alzheimer's disease and may even lead to shock. Currently, a large variety of food such as fruits, seafood, and staples i.e. potato endure a large risk to

[*] harrisontang168@outlook.com

Third International Conference on Biological Engineering and Medical Science (ICBioMed2023), edited by Alan Wang, Proc. of SPIE Vol. 12924, 129241Z
 · 0277-786X · doi: 10.1117/12.3013202

exposure under mercury ions. The World Health Organization identifies the total limit of mercury ions in food for safe consumption is at 3 mg/kg [12]. Therefore, attaining ultrasensitive detection for mercury (Hg^{2+}) ions is crucial to ensuring food safety. Traditional methods of detecting Hg^{2+} ions include luminescence and colorimetry: Colorimetry is the most common method for detecting mercury ions in food but exhibits low detection sensitivity, while luminescence is heavily dependent on large-sized detection machineries thus limiting the convenience for detection. These processes are highly complex and concludes results of lower sensitivity as compared to contemporary technologies [13]. In view of this, a method with high sensitivity, accuracy, and rapidity for measuring harmful substances in food is urgently required.

ECL detection technology combines electrochemistry [14] with luminescence [15] by identifying electrochemical properties of target substances, making detection highly sensitive (10^{-12} mol/L as the limit of detection [16]), accurate, easily integrated, and with low background interference. ECL detection techniques [17], such as potentiometric titration [18] in ECL carbon monoxide sensor, glucose sensor, and DNA sensors [19], are widely applicable in biosensors and improvement of component technologies. However, challenges still exist in ECL detection. For the detection of trace analytes, signal amplification is required to detect the target substance due to the weak ECL response. DNA cyclic amplification [20], representing a common traditional signal amplification technique, is widely investigated in food analysis. Nevertheless, interference sequences similar with the target substance's sequence that generate interference signals affect detection processes along the complex stages in modification of heating, chain propagation, and cooling [21]. This results in less efficiency with high false-positive rates. Therefore, the development of a novel signal-enhanced ECL technique with high efficiency is essential to improve the detection performances of the biosensor [22] in measuring Aflatoxin concentration.

Therefore, a method with high sensitivity and accuracy for measuring Salmonella pathogenic bacteria is urgently required [23]. Recently, the quasi-photonic crystal structure [24] was reported to increase the number of luminescent molecules with light-scattering signal amplification and exhibited better detection abilities, which effectively increase ECL detection capabilities [25]. Furthermore, photonic crystals embedding with gold nanoparticles in polystyrene nanomembrane can spontaneously amplify emissions and limit light propagation losses during detection [26]. This helps to increase detection accuracy and signal sensitivity. Thus, photonic crystals can be used as a favorable substrate applied in ECL signal amplification technologies. Currently, ECL biosensors for common food-borne harmful are limited in scope, lacks detection sensitivity, and possesses low accuracy. Thus, an ECL biosensor that is highly selective, sensitive, and efficient is required for the detection of multiple common food-borne harmful substances. Herein, an ultrasensitive biosensor for food-borne harmful substances is developed for the detection of Aflatoxin B1, Salmonella bacteria, and Mercury (Hg^{2+}) ions using TiO_2 PhC as enhanced substrate [27], CdS quantum dots as the emitter, and different selective methods as the experimental basis [28]. The photonic crystal substrates [29] can amplify the ECL biosensor signal to increase the luminescence efficiency. In the experiment, TiO_2 PhC [30] were fabricated on indium-tin oxides first through vertical deposition to obtain a mono-layer polystyrene opal structure and then immerse the TiO_2 PhC precursors in a sol-gel process to create a 3-D multi-aperture, ordered TiO_2 PhC inverse opal structure [31]. Next, the CdS quantum dots [32] are modified on the TiO_2 PhC inverse opal structure. The whole structure serves as the working electrode, with Pt threads as the counter electrode and Ag/AgCl as the reference electrode to establish a three-electrode system for ECL detection [33].

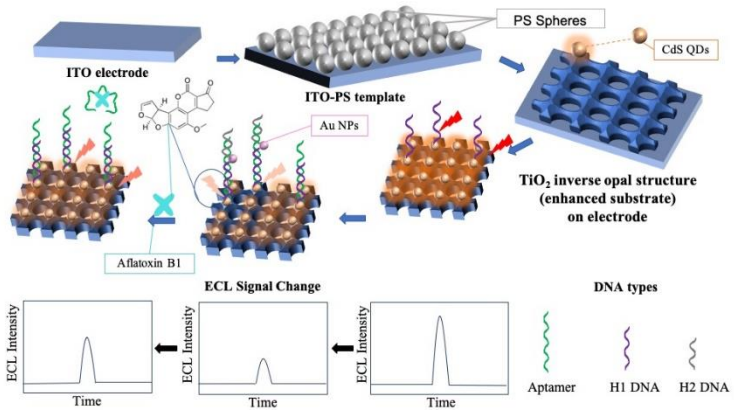

Scheme 1. Scheme illustration of the ECL biosensor for detection of Aflatoxin using TiO_2 as enhanced substrate with the "On-off-on" system.

The modification retrieval of the H1 DNA on the TiO_2 PhC inverse opal structure [34] surface and modification of Bovine Serum Albumin on the electrode surface helps to block the active sites on the electrode surface. Then, the aptamer is modified onto the electrode surface through DNA hybridization with H1 DNA. Gold nanoparticles (NPs) were introduced on the electrode by the nucleotide-base complementary pairing between H2 DNA and the Aflatoxin aptamer, which quenches the ECL signals of the CdS quantum dots [35]. Finally, in the presence of Aflatoxin B1, the Aflatoxin connects to the aptamer through specific DNA hybridization, which leads to the separation of Gold NPs away from the electrode. Under this circumstance, the ECL signal of CdS quantum dots recovers and the off-on detection strategy of Aflatoxin B1 was constructed [36]. A linear relationship between ECL signal strength and Aflatoxin B1 concentration can be established [37]. To determine Aflatoxin B1 concentration in crunched peanut samples [38], this research showed an ultrasensitive ECL biosensor for detecting Aflatoxin B1 which offers a new venue for monitoring the Aflatoxin B1 concentration in food.

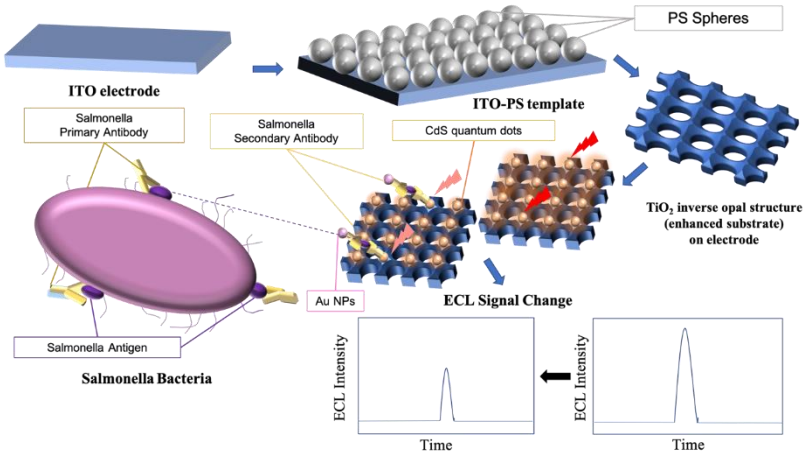

Scheme 2. An illustration of the constructed ECL biosensor for detection of Salmonella bacteria using TiO_2 as enhanced substrate with sandwich immunoassay.

The modification retrieval of the primary antibody on the TiO_2 PhC inverse opal structure surface and modification of Bovine Serum Albumin on the electrode surface helps to block the active sites on the electrode surface. Finally, in the presence of Salmonella bacteria, the Salmonella antigen connects to the primary antibodies through the antigen-antibody complex's specificity. The secondary antibodies, with gold nano-particles embedded, on the electrode surface quenches the CdS quantum dots' ECL luminescence, so a linear relationship between ECL signal strength and Salmonella concentration can be established.

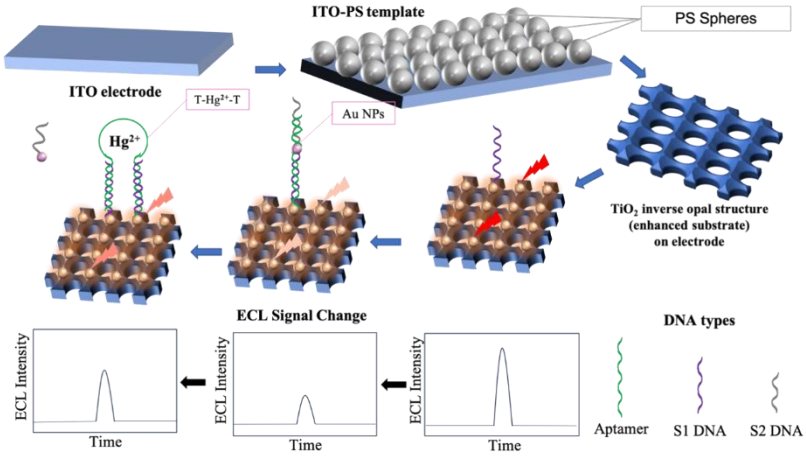

Scheme 3. An illustration of the constructed ECL biosensor for detection of Hg^{2+} ions using TiO_2 as enhanced substrate with T-Hg^{2+}-T specific structure.

The S1 DNA on the CdS quantum dots, under the combination with S2 DNA, AuNPs are modified onto the electrode surface and quench the ECL emissions of CdS quantum dots. With Hg^{2+} in place, Hg^{2+} will complimentarily bind with the S1 DNA via T-Hg^{2+}-T structure and consequently, AuNPs on an end of the S2 DNA is detached from the electrode surface. The ECL signal intensity recovers and the mercury Hg^{2+} ion concentration can be derived from the signal strength. For the 3 categorized target substances, a linear relationship between ECL signal strength and harmful food-borne substance concentration can be established.

2. METHODS

2.1 Materials and Instruments:

ECL Biosensor Reagent Kits and Consumables: 10X PBS buffer solution, Bovine Serum Albumin (BSA), Cysteine, 1% $HAuCl_4$ solution, EDC/NHS coupling agent, Mercapto-ethylamine blocking agent (MCH), Millipore ultrapure water (Resistance: 18MΩ), tetrabutyl titanate, Ethanol, 300 nm polystyrene microsphere (PS), 3nm infrared-emitted CdS quantum dots [39], PDDA Cationic Surfactants, 5 nm size gold nanoparticles (AuNPs), centrifugal tube, pipette tip, disposable gloves, plastic petri dish, beaker, glass petri dish, Salmonella surface monoclonal antibody Ab1, Salmonella surface monoclonal antibody Ab2, Aflatoxin H1 DNA, Aflatoxin H2 DNA, Aflatoxin B1 aptamer (APT), Mercury Hg^{2+} ion S1 DNA, Mercury Hg^{2+} ion S2 DNA, Mercury ions (Hg^{2+}), Aflatoxin B1, Salmonella bacteria, Sodium Citrate

Table 1. Aflatoxin DNA sequences of the ECL biosensor.

DNA Name	DNA Sequence
H1 (first DNA modified on the CdS quantum dots)	5'– NH_2 – ACAGAGAGACAACACGTGCCCAAC
APT	GTTGGGCACGTGTTGTCTCTCTGTGTCTCGTGCCCTTCGCTAGGCC
H2 (DNA modified on gold NPs)	GGCCTAGCGAAGGGCACGAGAC – SH – 3'

Table 2. Hg^{2+} DNA sequences of the ECL biosensor.

DNA Name	DNA Sequence
S1	5'– NH_2-C_6-TTAGAACAACAAGGAAGATT
Aptamer	GAACACCCCCTTCTTCTTCCTTGTTGTTC
S2	TTAAAGAAGGGGGTGTTCATT-C_6-SH-3'

Experiment Equipment: Millipore ultrapure water machine, CHI660C electrochemical workstation, Pt counter electrodes and Ag/AgCl reference electrode making up the Three-Electrode system, ECL analyzer detector, Autolab electrochemical impedance tester, UV-vis spectrophotometer, emission spectrometer, Zeiss scanning electron microscope, ITO glass cutter, Pipettes, ITO glass [40] (Resistance: 10 Ω), Photomultiplier tube (PMT set at -600 V)

3. EXPERIMENTAL STEPS

3.1 The Preparation of Photonic Crystals

On the ITO, PS microspheres [41] are precipitated through the vertical deposition method. An ITO glass with dimensions of 1.5 cm by 2 cm is cut by an ITO high-precision glasscutter that function as working electrodes in the experiment. The PS emulsions of 10% solid content are diluted to a 0.5% solid content of 5 mL volume [42] After that, the plasma cleaner cleans the ITO electrodes [43]; the ITO glass is vertically placed into the 5mL emulsion of 0.5% solid content and dried in the drying oven at 55℃ for 36 hours, so a monolayer PS opal structure was obtained.

3.2 Fabrication of the TiO_2

Tetrabutyl titanate and alcohol solution are first mixed at a one-to-three ratio. 20 mL of mixed solution is used as TiO_2 precursor [44], for which the prepared ITO-PS opal structure is immersed 3 times at 5 minutes each. Then, alcohol is used to rinse the electrode; the electrode is dried and put into a high-temperature muffle furnace of 550℃ for 6 hours of

calcination. After calcination, a three-dimensional, multi-aperture ordered anatase TiO_2 inverse opal structure [45] is formed and reserved as the electrode for later usage.

3.3 Electrode surface morphological characterizations

The prepared TiO_2 inverse opal electrode is titled from 1-9 and stacked onto the specimen holder of the SEM [46] via conducting resin. Then, the electrode is placed into a vacuum chamber and exerted upon electron beams. After morphological test by the SEM, TiO_2 electrode surface and lateral side characterizations can be observed.

3.4 Preparation of the Electrochemiluminescence sensor

10mL of PDDA aqueous solution [47] with 0.5% NaCl was used to dilute the CdS quantum dot sol 5 times. Another 10 mL was applied to rinse the TiO_2 inverse opal electrode in PDDA aqueous solution and CdS quantum dot solution 5 times for 1 minute each so the CdS quantum dots can be completely modified onto the TiO_2 inverse opal structure. The TiO_2-CdS electrode structure is dispensed with 200 μL cysteine [48] of 1% density. Through the formed disulfide bond, cysteine can be modified. Then, the TiO_2-CdS electrode is rinsed into a 10 mL EDC/NHS-PBS buffer solution of density 20 mg/mL to functionalize the carboxyl groups on the electrode surface. Subsequently, The TiO_2-CdS electrode is rinsed into a specific primary molecule (antibody/DNA) paired with the target substance and smeared with 2% BSA-PBS buffer solution onto the electrode surface. Thus, BSA [49] is modified onto the electrode surface, sealing off the active sites on the electrode surface.

3.5 The characterization of Electrode Electrochemiluminescence biosensor

After modification, the TiO_2 inverse opal – CdS quantum dot structure is used as the working electrode, the Pt thread is the counter electrode, and Ag/AgCl is the reference electrode, thus establishing a three-electrode system. The voltage is set at -1.5~0 V and a scanning speed of 0.1 V/s to record the electrochemical signals on the electrode.

3.6 Aflatoxin B1 concentration in food and analysis of Aflatoxin B1 DNA

Aflatoxin B1 with different concentrations (200, 50, 10, 5, 2, 1 ng/mL) in PBS buffer solution is drop-coated onto the surface of the TiO_2 inverse opal electrode surface and incubated for 2 hours under 37 ℃. The MPI-E electrochemiluminescence analyzer detector helps to detect the intensity differences of electrochemiluminescence signals. The target substances' secondary antibodies or DNA and/or aptamers are then modified, in this case H2 DNA and aptamer for Aflatoxin B1. Finally, 10 g of peanut samples are crumbled and immersed into 0.1 mol/L PBS buffer for detecting the ECL signals.

3.7 Salmonella bacteria concentration in food and analysis of Salmonella bacteria antibodies

Salmonella bacteria with different concentrations (500, 200, 50, 20, 10 mL^{-1}) is rinsed into the PBS buffer solution and limited [50] to around 250. Similarly, the MPI-E ECL analyzer detector helps to detect differences in signal intensity. Through the antigen-antibody complex's specificity, Salmonella is connected to the primary antibodies. The electrode modified with the Salmonella antigen is then rinsed with the secondary antibody, while the electrode surface is dispensed with 5 nm gold nanoparticles to quench the electroluminescence of CdS quantum dots. Finally, the milk samples are diluted and mixed into the PBS buffer solution to detect the ECL signals.

3.8 Mercury (Hg^{2+}) ions in water and analysis of the T- Hg^{2+}-T structure

S1 DNA is modified onto the CdS quantum dots via EDC-NHS coupling. The mercury ion's aptamer binds to S2 DNA. Hg^{2+} ions with different concentrations (1 pmol, 10 pmol, 100 pmol, 1 nmol, 10 nmol) is rinsed into the PBS buffer solution. The density of the S1/S2 DNA strands are 1umol/L. The MPI-E ECL analyzer detector helps to detect differences in signal intensity. Through the Thymine-Mercury ion binding specificity, mercury ions are connected to the thymine nucleotides on the aptamers added. The S2 DNA strand then added binds to AuNPs, dissociating latter with the electrode after such binding. Finally, the water samples are mixed into the PBS buffer solution to detect the ECL signals.

4. RESULTS AND DISCUSSION

4.1 Characterization of Polystyrene (PS) template and TiO_2 inverse opal

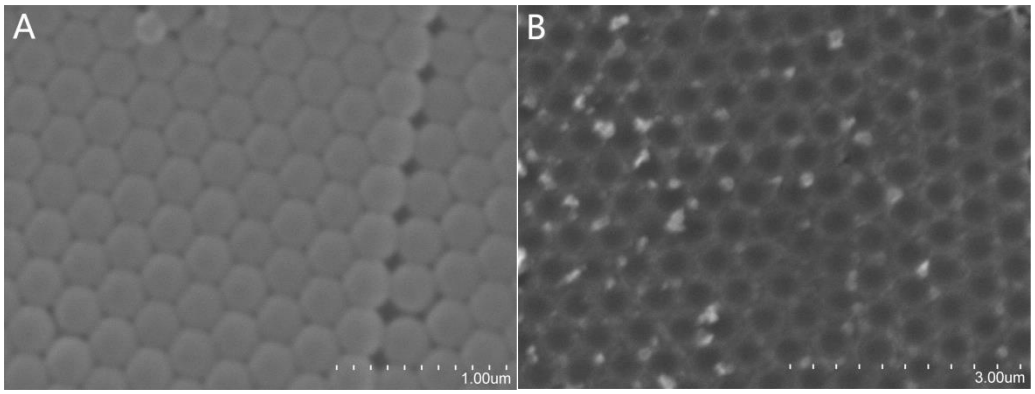

Figure 1. A: SEM morphological characterization of the PS template on ITO electrode, scale bar: 1 μm. B: SEM morphological characterization of the TiO_2 Inverse Opal Structure, scale bar: 3 μm.

The mono-layer, opal-structure template characteristics of the prepared material after modification with ITO glass slides can be shown from the SEM image. The template has high uniformity, small gaps, and no cracks, reflecting a successful preparation of the polystyrene of the template. The diameter of a single modified PS sphere is approximately 0.30 μm, which is equal to the dimensions of the TiO_2 inverse opal enhanced substrates. The PS template in ordered forms placed within the working electrode is used throughout the experiment.

The multi-layer characteristic of the TiO_2 inverse opal structure can be shown from different apparent levels of its apertures, which is organized in analogous circular shapes along the template. After calcination, the Ti-OH bands are weakened and oxygen vacancies are formed though no phase change occurred during the rapid temperature increase. The inverse opal structure has cavities and dimensions of 0.3 μm diameter. The structure is closely immersed into the PS template, which reflects that it's a good anatase structure. The template remains highly uniform under a large dimension and is closely aligned in a comb-shaped structure. TiO_2 inverse opal also has a large surface area that can be later used for effective modification of CdS quantum dots and respective antibodies.

4.2 Morphological Characterization and Spectrometry of Gold NPs

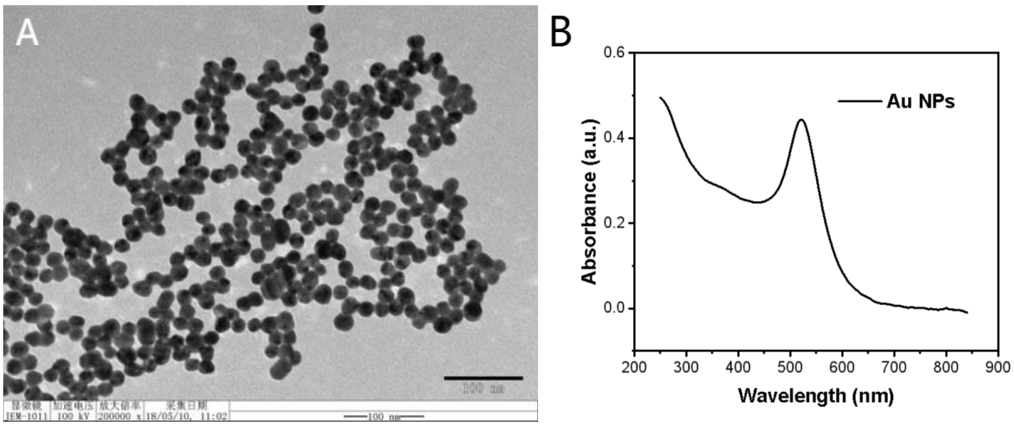

Figure 2. A: SEM morphological characterization of Gold Nanoparticles, with a scale bar of 100nm. B: UV-Vis absorption spectrum of Gold NPs.

As shown in figure 2A, The Gold NPs have an average diameter of 15 nm. From figure 2B, the Gold NPs have higher absorption spectrums (abs) around 250 nm and 530 nm, with the former wavelength approaching the UV spectral region and the latter wavelength because of local surface plasmon resonance. The absorption peak is 530 nm around green visible spectrum, which overlaps well with the emission spectrum of the CdS quantum dots, making it an affective micro-particle for quenching the ECL signals. The structure has uniform characterization as an effective arrangement for its attachment to CdS quantum dots.

4.3 Electrochemical Impedance Spectroscopy

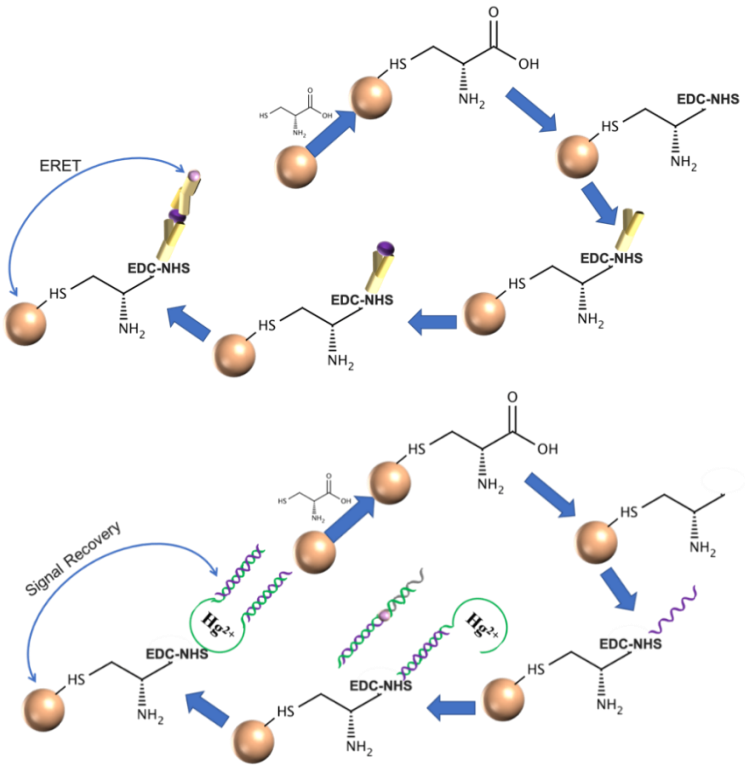

Scheme 4. The incubation steps of the CdS quantum dots modified on the TiO_2 inverse opal structure, for salmonella bacteria and mercury ions.

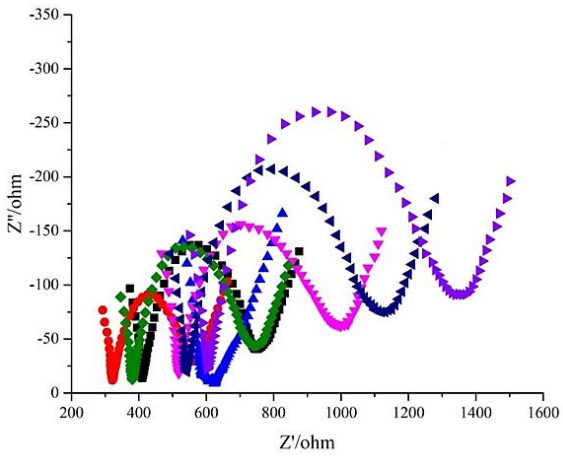

Figure 3. The EIS values of the TiO_2 ECL biosensor during each modification step. Electrochemical Impedance Spectroscopy was characterized by Autolab electrochemical work station. The detection solution was 0.1M KCl containing 5 mM of $K_3Fe(CN)_6$ and $K_4Fe(CN)_6$. The frequency was from 100 kHz to 0.1 Hz.

It can be observed that the ITO EIS has obviously increased after vertical deposition of TiO_2 inverse opal structure. After modifying CdS quantum dots, EIS continuously increased. The semicircle curves refer to the incubation process of the CdS quantum dots. The red curve represents the TiO_2 electrode's initial state. The bright blue curve represents the TiO_2 electrode modified with CdS quantum dots, apparent from the substantial increase in EIS value and symbolizes the

successful modification of CdS quantum dots onto the electrode surface. The black curve represents the TiO_2-CdS electrode modified with cysteine. The green curve represents the TiO_2-CdS electrode modified with cysteine and EDC-NHS. The light pink curve represents the EIS after modification of primary antibody onto the TiO_2-CdS electrode. The dark blue curve represents the EIS change after modification of Salmonella bacteria antigen onto the TiO_2-CdS electrode. Lastly, the purple curve represents the TiO_2-CdS electrode modified with secondary antibody and AuNPs. The EIS change throughout the process is directly proportional to the modification of substances onto the TiO_2 electrode, meaning that the electrode is successfully constructed for detection.

4.4 Characteristics of Electrochemistry and ECL properties

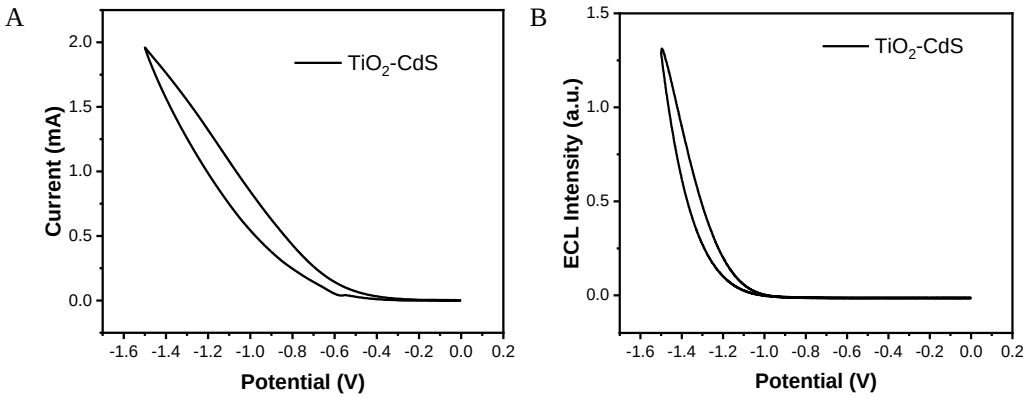

Figure 4. A Current-Potential curve (A) and ECL Intensity-Potential curves (B) of TiO_2-CdS electrode on the ITO glass substrate. Cyclic voltammetry scanning was tested in the voltage range of -1.5~0 V with scanning speed of 0.1 V/s. PMT voltage was set at -600 V. The co-reactant was $K_2S_2O_8$.

In figure 3a and 3b, the Electrochemical characteristics and ECL properties are shown in the relationship between Current and ECL intensity versus potential. Figure 3a reaches the peak current strength of 1.2 mA at -1.5V given the voltage range set from -1.5 ~ 0 V with scan rate of 0.1V to record the properties. The strongest detection signals can be seen from this peak. The sensitivity increases as ECL intensity in detection rises to a stable level. After several excitation cycles of rapid increase towards high sensitivity, the ECL intensity reaches a stable level around -1.3, signaling the ECL detection activities.

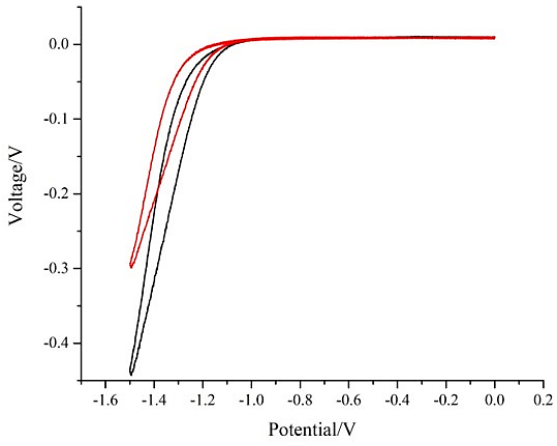

Figure 5. The ECL intensity before and after the modification of Salmonella and the secondary antibody – AuNPs complex. The experiment was conducted on the potential of -1.5~0 V. PMT voltage was set at -600 V. The co-reactant was $K_2S_2O_8$.

Before the modification of Salmonella bacteria, the TiO_2-CdS electrode was modified with primary antibody and the ECL signal slightly decreased the value of -0.45 V due to the decrease in conductivity and an increase of the steric hinderance. Through the specific binding between Salmonella surface antigen and the primary antibody, the Salmonella bacteria is modified onto the electrode surface, which offered the active sites for the subsequent modification of

secondary antibody and AuNPs. Due the high quenching efficiency of AuNPs against CdS quantum dots, ECL signal decreased to -0.3 V, suggesting that the sensor on the electrode surface has a favorable signal response.

4.5 ECL spectrometry of CdS quantum dots

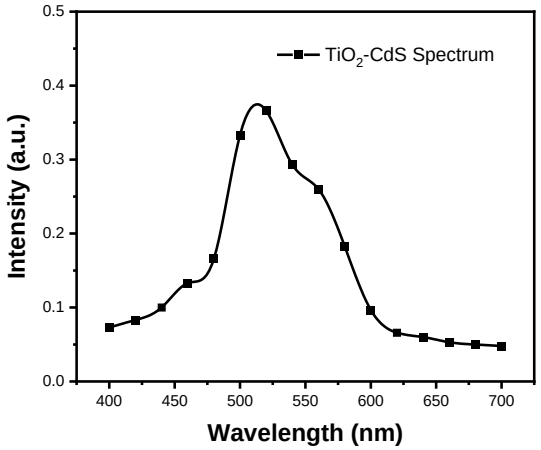

Figure 6. The ECL emission spectrum of the CdS quantum dots modified at the TiO_2 photonic crystals.

The ECL spectrometry is conducted with detection filters of 20 nm intervals. The spectrometry's initial detection wavelength is 400 nm and ranges from 400 to 700 nm. The CdS quantum dots luminescence wavelength is 518 nm which has an acceptable spectrometric overlap with the UV-vis spectrum of Gold NPs, 530 nm. This special overlap results in significant quenching of CdS quantum dots and increases the sensitivity of the biosensor.

4.6 Detection Principles of the ECL biosensor

$$CdS + e^- \rightarrow CdS^{\bullet -}$$

$$S_2O_8^{2-} + e^- \rightarrow SO_4^{\bullet -} + SO_4^{2-}$$

$$CdS^{\bullet -} + SO_4^{\bullet -} \rightarrow CdS^* + SO_4^{2-}$$

$$CdS^* \rightarrow CdS + h\nu$$

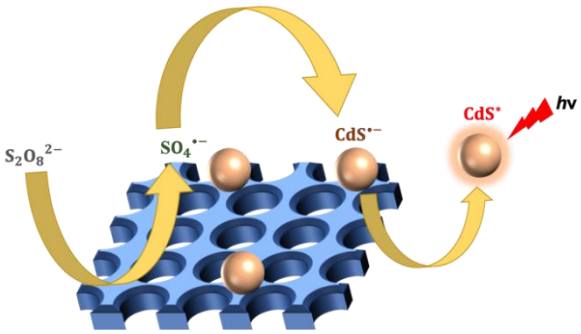

Scheme 5. The mechanism of the ECL emission enhanced by TiO_2 substrate.

First, the CdS quantum dots are reduced to anion radicals under the negative scan from 0~-1.5 V of the electrode. Meanwhile, the $S_2O_8^{2-}$ anions are reduced to anion radical $SO_4^{\bullet -}$, a strong oxidizing agent. The generated anion radicals can be oxidized by anion radical $SO_4^{\bullet -}$ to produce unstable CdS^*, which then returns to ground state and emits light.

TiO_2 inverse opal structure as an PhC structure has a considerably large surface area and can provide more active sites for absorption of CdS quantum dots, thus increasing the modified number of CdS quantum dots on the TiO_2 structure surface. Because TiO_2 has a relatively large electrochemical activity, it can enhance the ECL speed of the CdS quantum dots. Besides, as a PhC structure, TiO_2 structure can improve the transition rate of through the PhC induced electromagnetic field, increasing luminescence of the CdS quantum dots.

4.7 Detection Performances of the ECL biosensor

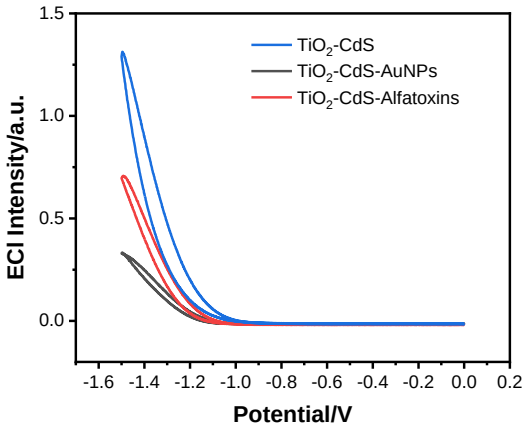

Figure 7. The potential-ECL intensity curve of TiO_2-CdS electrode. The black curve exemplifies the TiO_2 electrode before Gold NPs are modified. The blue curve represents the TiO_2 electrode modified with Aflatoxin B1. The red curve denotes the TiO_2 electrode modified with the Gold NPs.

Before the modification of Gold NPs, the strongest experimental signal of 1.33 is exhibited from ECL biosensors during the "on" stage when H1 DNA undergo specific attachment to Aflatoxin B1 without considerable interference. The CdS quantum dots' luminescence are effectively quenched by the Gold NPs and the system is turned off as H2 DNA containing the Gold NPs hybridize with H1 DNA on the electrode. Thus, after partial quenching, the ECL signals is reduced towards low levels of 0.32. As Aflatoxin B1 binds with the aptamer, the ECL signals are recovered as shown in 0.71 signal intensity and applied for graphing the linear relationship between ECL signal intensity and Aflatoxin B1 concentration.

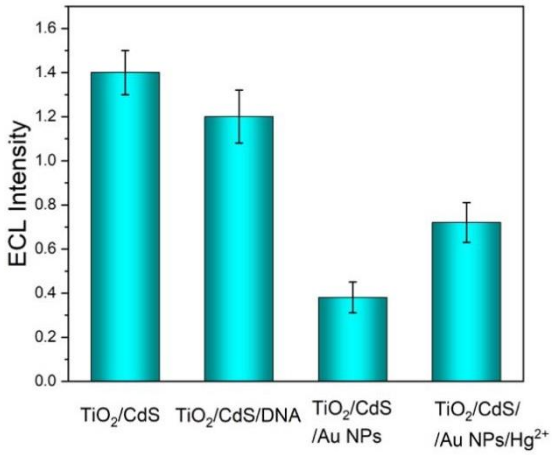

Figure 8. The ECL intensity of TiO_2-CdS electrode itself and with modification of Hg^{2+} S1 DNA, AuNPs, and mercury ions.

An ECL intensity of 1.4 is exhibited from the TiO_2-CdS electrode. The ECL intensity is decreased to 1.2 when mercury ion S1 DNA is modified onto the electrode. After AuNPs are binded with the S2 DNA, which is hybridized with mercury ion aptamer that is attached to the S1 DNA on the electrode, ECL intensity is significantly decreased to 0.4 due to the quenching effect upon CdS quantum dots. As the T-Hg^{2+}-T is formed between the aptamer and S1 DNA modified onto the electrode with Hg^{2+} ions, ECL signal intensity is recovered to 0.7. A successful ECL detection mechanism can be shown from such changes.

4.8 Optimization of the experiment conditions

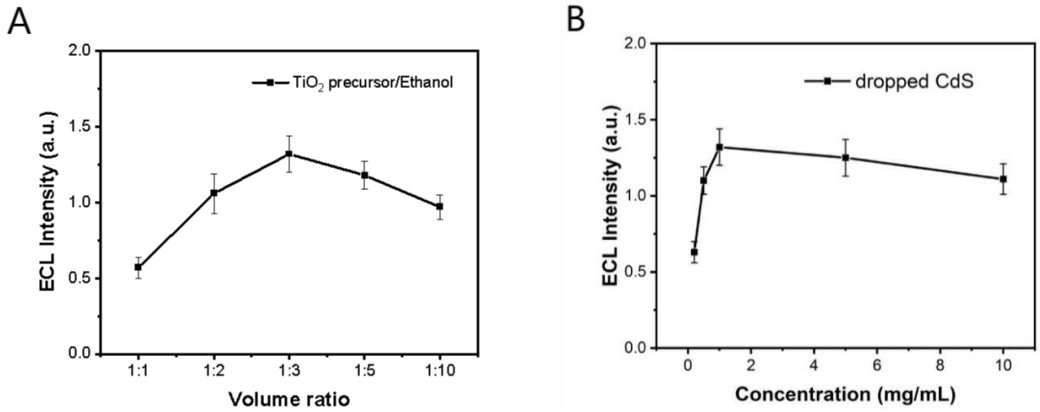

Figure 9. A: TIO_2 precursor concentration in relations to ECL intensity. B: CdS quantum dots concentration versus ECL intensity.

In this experiment, the volume ratio of TiO_2 precursor/Ethanol and concentrations of dropped CdS quantum dots are optimized. As shown in figure 9A, when TiO_2 precursor and Ethanol solution reach a 1:1 volume ratio, the ECL intensity is weaker because the precursor concentration is over-excessive leading to the failure of TiO_2 inverse opal structure formation. When TiO_2 precursor and Ethanol solution reach a 1:3 volume ratio, the peak ECL intensity thus peak signal strength is exhibited. When TiO_2 precursor and Ethanol solution reach a 1:10 volume ratio, the TiO_2 precursor concentration is minimal, leading to an extremely thin TiO_2 inverse opal structure and hindering the signal. The dropped CdS quantum dots exhibit the peak ECL intensity and thus luminescence around a concentration of 1.2 mg/mL with a suitable amount modified. Because of the steric hindrance effect of 5 mg/mL CdS concentration levels, ECL signal intensity decreased. Therefore, dropped CdS quantum dots with concentration of 1.2 mg/mL and volume ratio of 1:3 for TiO_2 precursor to Ethanol are selected as the optimal conditions.

Table 3. Concentration optimization in Aflatoxin B1 detection.

Trial	Concentration (μM)	Final ECL intensity (a.u.)
1	0.1	0.63
2	0.2	0.58
3	0.5	0.55
4	1	0.32
5	2	0.47

Table 4. Concentration optimization in Salmonella detection.

Trial	Concentration (μg/ml)	Final ECL intensity (a.u.)
1	0.1	0.39
2	0.2	0.37
3	0.5	0.34
4	1	0.3
5	2	0.33

Table 5. Concentration optimization in Mercury ion detection.

Trial	Concentration (μM)	Final ECL intensity (a.u.)
1	0.1	0.66
2	0.2	0.47
3	0.5	0.49
4	1	0.38
5	2	0.43

In Table 4 and Table 6, when the DNA concentration is increased from 0.1 μM, the concentration of incubated DNA on the electrode is increased. Thus, the concentration of aptamer hybridized onto the electrode is increased and the corresponding concentration of AuNPs is increased by binding to the aptamer via H2 and S2 DNA for Aflatoxin B1 and Mercury ion respectively. The quenching effect is increased, and the ECL intensity is decreased. When the optimal concentration of 1 μM is reached in both cases, continuous increase of the DNA concentration makes the modifications on electrode surface crowded. This leads to the decrease in concentration of incubated AuNPs and the quenching effect is diminished.

In Table 5, when the concentration of the antibody is increased from 0.1 μg/ml to the optimal level of 1 μg/ml, the antigen and pathogenic bacteria amount modified on the electrode is increased, which increases the steric hindrance. Thus, concentration of incubated AuNPs is increased, the quenching effect is amplified respectively. However, when the antibody concentration is increased from the optimal level, the arrangements of the antibody on the electrode surface becomes disorganized and uneven. As result, the concentration of incubated antibodies and pathogenic bacteria decreases and the quenching effect is diminished.

4.9 Stability of the Electrode

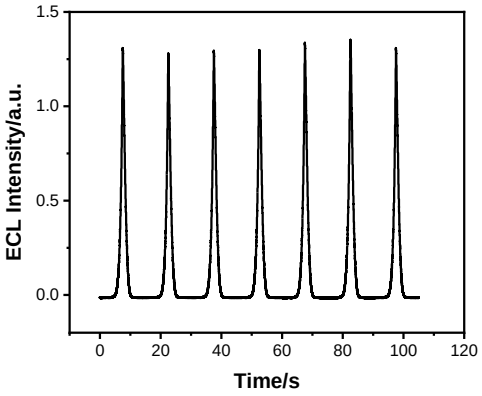

Figure 10. ECL Stability curves of TiO_2-CdS electrode on the ITO glass substrate. Cyclic voltammetry scanning was tested in the voltage range of -1.5V~0V with scanning speed of 0.1V/s. PMT voltage was set at -600V. The co-reactant was $K_2S_2O_8$.

After repeatedly measuring the ECL intensity of detection under the potential range, curves with similar trends are shown on the figure, with multiple overlaps and all reaching the maximum ECL Intensity of 1.25~1.3 a.u. in time intervals of approximately 12.5 s after the first ECL intensity peak near 7.5 s. Also, The ECL intensity has less than 1% of uncertainty and a high stability during detection. Thus, the stability of the electrode can be shown through the highly sensitive detection abilities and stable performance of intensity at an accurate potential range.

4.10 Linear relationship of the biosensor

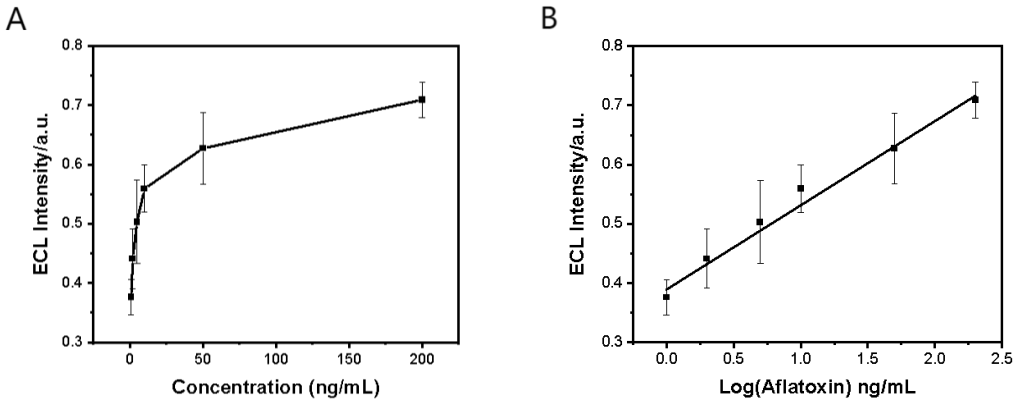

Figure 11. (A) The ECL intensity at different concentrations of Aflatoxin B1s (1, 2, 5, 10, 50, 200 ng/mL). (B) The linear relationships of the ECL biosensor.

Under the optimal conditions, the biosensor exhibits superior detecting performances due to the specific recognition between Aflatoxin and its aptamer and the high quenching efficiency of Gold NPs to CdS quantum dots. As shown in figure 11A, the ECL intensity changes with concentrations of Aflatoxin ranges from 1 ng/mL to 200 ng/mL. The linear relationships are exhibited in figure 11B, with the equation of I=0.142c+0.389 (I represents the ECL intensity of the biosensor while c represents the concentration of Aflatoxin B1). The detection limit was evaluated as 1 ng/ml which shows good detection sensitivity.

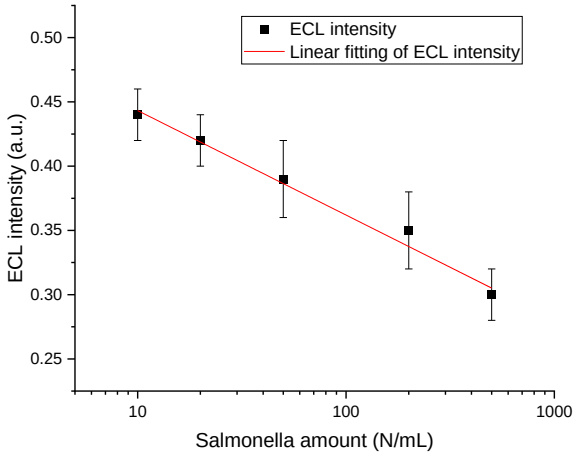

Figure 12. The ECL detection intensity varies with the change of Salmonella bacterial concentration in the range of 10N/mL to 500N/mL.

In the presence of Salmonella bacteria, the specific binding of antigen on antibody makes possible the modification of AuNPs onto electrode surface. Subsequently, an ultrasensitive biosensor was constructed and used in the detection of Salmonella bacteria concentration. Figure 12 displays the ECL detection intensity's variation with the change in Salmonella bacterial concentration in the range of 10~500 N/mL. With the increase in concentration of Salmonella bacteria, the ECL detection intensity gradually decreases, and a linear relationship between the two is established. The equation of the best-fit line is I=-0.081*lgc* + 0.524 (I represents the ECL signal intensity of the biosensor while *lgc* represents the concentration of Salmonella in the detection samples). The limit of detection is 10 Salmonella bacteria, which shows great promise in food safety analysis.

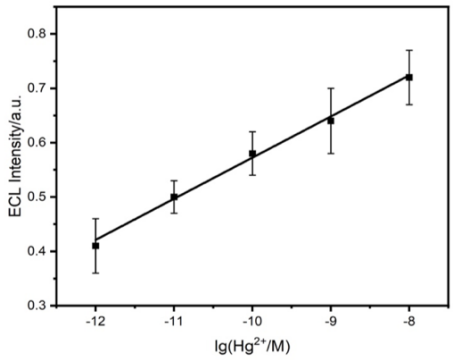

Figure 13. The ECL detection intensity varies with the change of mercury ion concentration in the range of 10^{-12} to 10^{-8} Hg^{2+}/M.

In the presence of mercury ions, aptamer binding modifies the AuNPs onto the electrode surface. The biosensor can be constructed upon the principle of T-Hg^{2+}-T (T for thymine nucleotide) specific structure formation, and Figure 13 shows the ECL intensity's change with the change in concentration of mercury ions in the range of 10^{-12} to 10^{-8} mol/L. With the increase in concentration of mercury ions, ECL intensity increases as CdS luminescence recovers, thus a linear

relationship is established. The equation for best fit line is I=0.076*lgm* + 1.329. (*lgm* represents the concentration of mercury ions in target samples), while detection limit is 10^{-12} mol/L.

4.11 Aflatoxin B1 detection in peanut samples

Table 6. Real sample detection of Peanut using ECL biosensor.

Samples	Detected Concentrations (ng/mL)	Added Concentrations (ng/mL)	Found Concentrations (ng/mL)	RSD (%)
Peanut	0.00	2.00	2.03	4.3

In traditional methods of detecting aflatoxin B1 such as liquid chromatography, the detection limit of aflatoxin B1 is around 0.1 mg/kg for each toxin of B1, B2 [51], G1, and G2, while other techniques such as Raman scattering detection, detection limits can be reached towards 0.5 μg/L for Aflatoxin B1[52]. The detection time of Aflatoxin B1 in this research accounts for 15 minutes in total, while those of other techniques may be rapid in analysis even as to only 1 minute but have normal pace considering detection effiency. The detection stage is initiated by first ensuring the Aflatoxin B1 detection concentrations in a commercialized peanut product is zero. Regarding detection limits, the detection sensitivity of this Aflatoxin B1 DNA based method is extensive with a measured value of 2.03 ng/mL and relative standard deviation of 4.3%, differing only by 0.03 ng/mL from the actual concentration added. This can be compared to traditional methods such as liquid chromatography, which have high standard deviations topping 15% and long durations of 13 minutes to separate the 4 toxins (B1, B2, G1, G2) [53]. Overall, the multiple series of detection experiments result in similar values showing high detection accuracy.

4.12 Analysis of Salmonella concentration in milk samples

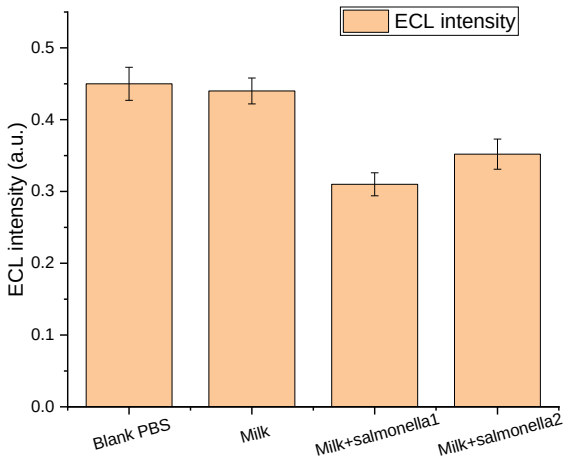

Figure 14. The ECL detection intensity with addition of 500 and 200 Salmonella bacteria for Salmonella sample 1 and 2 respectively.

To measure the practicability of the biosensor design, the detection of Salmonella bacteria in milk real sample was analyzed. Firstly, the milk samples were diluted ten times and dispersed in 0.1 mol/L PBS solution. The obtained milk samples were incubated at the electrode and for two hours. The milk sample, as compared to empty PBS samples, has few signal intensity changes. This demonstrates that there's few to none Salmonella bacteria in common milk samples. The Milk + Salmonella sample 1 with 500 Salmonella bacteria has a significantly lower detection intensity than Milk + Salmonella sample 2 with 200 Salmonella bacteria. This shows that the percent recovery is favorable, with few interferences from the milk sample during the detection of Salmonella Bacteria. The components in milk samples will not substantially affect detection results.

4.13 Analysis of mercury ions concentration in water samples

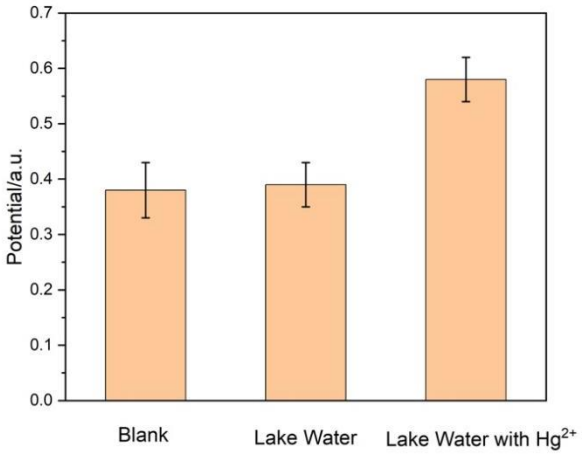

Figure 15. The ECL detection intensity with addition of mercury ions in the lake water sample.

The water solutions were first diluted and mixed into PBS buffer solution, while obtained water sample of 100 mL is retrieved via the pipette and incubated onto the TiO_2-CdS electrode for two hours. As result, the lake water has a slightly higher ECL intensity than the blank sample, showing that there is a low initial concentration of mercury ions in the lake water. However, when 1 mL of mercury ions is diluted to attain a mercury ion concentration of 10^{-10} mol/L, the ECL intensity significantly increases. This shows a favorable recovery rate and low interference of the lake water itself, which is mostly free of mercury ions, on the biosensor detection results.

4.14 Stability and Selectivity of the Electrode for detection of Salmonella: S. Aureus, Cholera, and E. coli

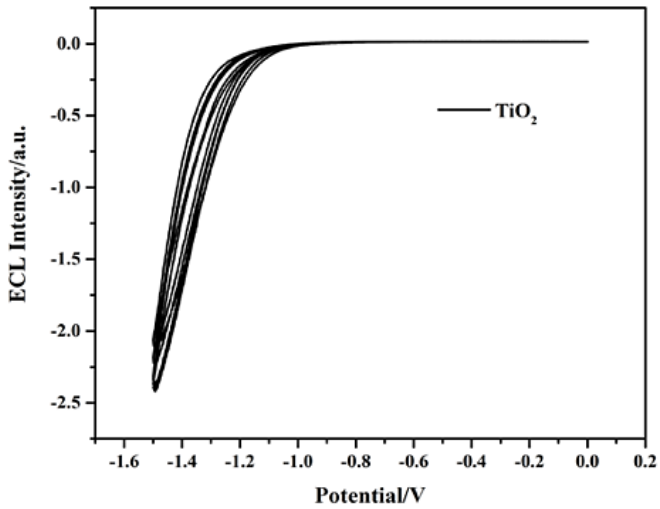

Figure 16. ECL Stability curves of TiO_2-CdS electrode on the ITO glass substrate. Cyclic voltammetry scanning was tested in the voltage range of -1.5~0 V with scanning speed of 0.1 V/s. PMT voltage was set at -600 V. The co-reactant was $K_2S_2O_8$.

After repeatedly measuring the ECL intensity of detection under the potential range, curves with similar trends are shown on the graph, with multiple overlaps and all reaching the maximum ECL Intensity in the potential range around -1.1~-1.0 V. Also, The ECL intensity has less than 1% of uncertainty and a high stability during detection. Thus, the stability of the electrode can be shown through the highly sensitive detection abilities and stable performance of intensity approaching zero at an accurate potential range.

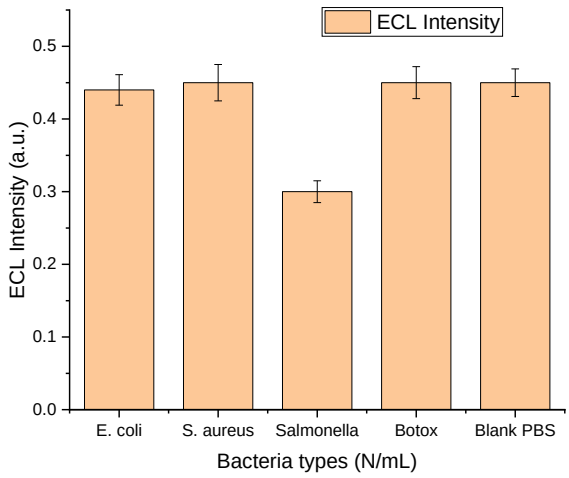

Figure 17. ECL signal intensities of different types of bacteria under detection.

In the process of selectivity detection, the same amount of 500 bacteria was used in the biosensor. The different types of bacteria, such as E. Coli, Staphylococcus Aureus, Salmonella Bacteria, and Clostridium Botulinum, were tested. The signal intensity of bacteria types besides Salmonella is nearly identical to that of the blank PBS solution. The detection intensity of Salmonella bacteria is significantly lower than the other bacteria samples, showing the favorable selectivity of the biosensor and less interference from other types of bacteria.

4.15 Selectivity of the Electrode for detection of mercury ions: Pb^{2+}, Cu^{2+}, and Zn^{2+}

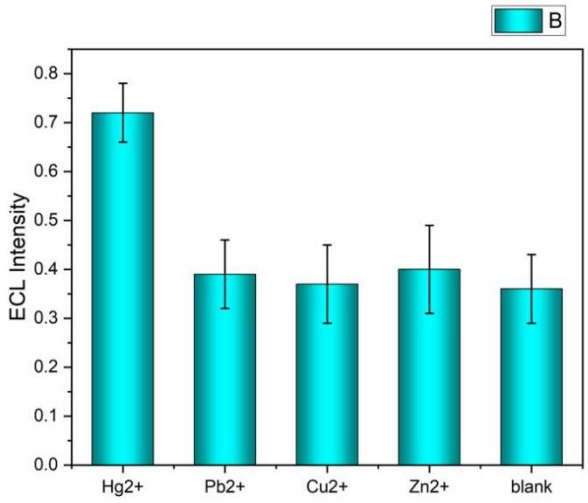

Figure 18. ECL signal intensities of different types of heavy metal ions under detection.

A concentration of 10^{-8} mol/L of mercury ions were used in the detection process, with other metal ions in presence such as lead, copper, and zinc ions along with a blank sample. The signal intensity of the other heavy metal ion samples is nearly same while those of mercury ions is significantly higher, reflecting high selectivity on detecting mercury ion concentrations.

4.16 Optimization Results and Detection of Aflatoxin B1 in POCT-ECL biosensor

Table 7. Different quenching particles tested for POCT-ECL biosensor.

Quenching Particle Type	Fc	Fc-SiO_2	Nafion-Rubpy	Pt	Au	Ag
Initial ECL Intensity	0.36	0.38	0.07	0.37	0.37	0.37
Final ECL Intensity	0.28	0.10	0.03	0.32	0.40	0.35
Quenching Efficiency	23%	74%	57%	14%	/	0.5%

Since the $Ru(bpy)_3^{2+}$-TPA coreactant ECL system is applied onto the POCT-ECL biosensor based on the novel TiO_2 inverse opal electrode, a new, optimal quenching particle suited with the new ECL liquid-state emitter $Ru(bpy)_3^{2+}$ is required to perform ultrasensitive detection of target analytes. By testing Ferrocene (Fc), Ferrocene-SiO_2, Nafion-Rubpy, Pt, Au, Ag, and other quenching particle's effect on the emitted ECL intensity before and after quenching, low quenching efficiency is exhibited from many particles due to spectrometric properties variances with $Ru(bpy)_3^{2+}$. The optimal particle is derived as Fc-SiO_2, which has a quenching efficiency of over 74%.

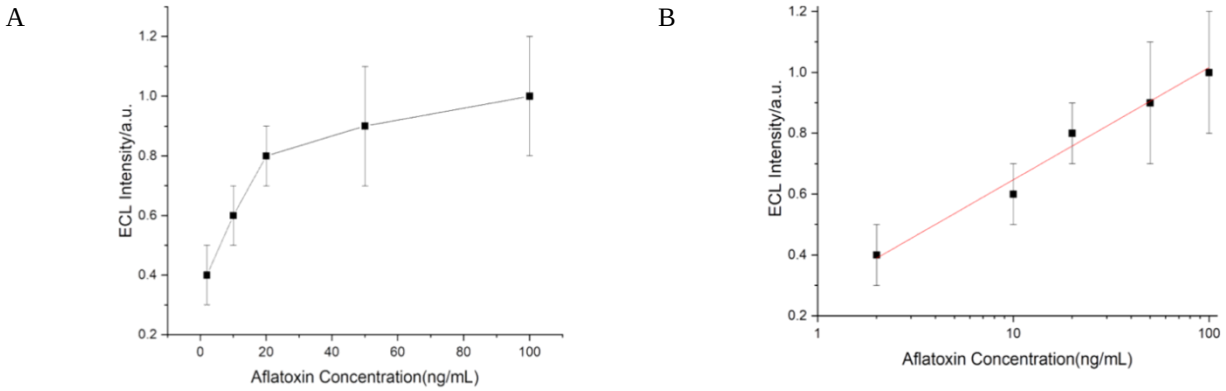

Figure 19. (A) The ECL intensity at different concentration of Aflatoxin B1s (1,10, 20, 50, 100 ng/mL) under detection in the POCT-ECL biosensor (B) The linear relationship of the POCT-ECL biosensor.

In the POCT-ECL biosensor, Aflatoxin B1 detection was tested through the developed novel aptamer sensing system utilizing highly efficient Fc-SiO_2 quenching particles in the $Ru(bpy)_3^{2+}$ coreactant ECL emission system. As shown in figure 19A, the ECL intensity changes when Aflatoxin B1 concentration ranges from 1 ng/mL to 100 ng/mL. With the log of concentration plotted on the X-axis, linear relationship is established between Aflatoxin B1 concentration and ECL intensity in figure 19B. The detection limit was 1ng/mL proving as favorable detection sensitivity as compared to the novel ECL biosensing system and conventional POCT methods.

5. APPLICATIONS

5.1 Prototype appearance and structure

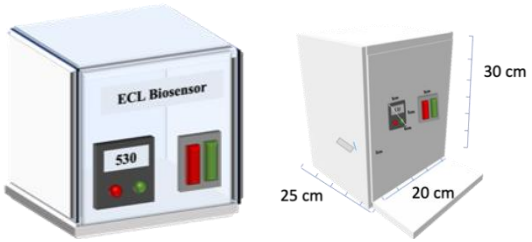

Figure 20. POCT-ECL biosensor prototype design.

The dimension of the biosensor is $20\,(width\ from\ front) \times 25\,(depth) \times 30(height)$ cm. The POCT-ECL biosensor designed for household usage is consisted of an LCD display screen and mode control in the front. The LCD display screen is used to display the signal intensity of the light meter, and the mode control is used to select the detection electrode used for food sample analysis. On the left-hand side, the sample input is an opening used for placing the electrode piece on the detection sample and electrode holder that is located on the interior. The interior of the prototype is consisted of a light meter, which is used for measuring light intensity of ECL emissions, directly above the sample holder with two batteries of potential difference 1.5 V each located on the right-hand corner.

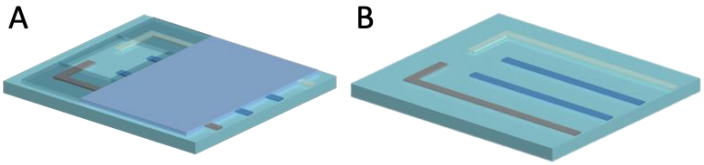

Figure 21. POCT-ECL biosensor integrated electrode piece.

In 21A, two layers of Polydimethylsiloxane (PDMS) are covered onto the electrode piece. One layer is used as a surface covering, while the other is used as a liquid reservoir for the electrolyte. In 21B, the left L-shaped electrode strip is made of Pb, and the right corresponding electrode strip is the Ag/AgCl reference electrode. The two electrodes in the middle are working electrodes made of ITO and TiO_2 PhC enhanced substrates.

5.2 Detection performance

Figure 22. POCT-ECL prototype model.

To begin with, solutions of $Ru(bpy)_3^{2+}$, TPA, and PBS buffer solutions are dropped and mixed into the liquid reservoir using the pipette. Then, the liquid reservoir is placed onto the corresponding electrode tray. When the power is turned on and the electrode is supplied with electricity, ECL light emissions is produced from the light reservoir which can be accessible to the light meter. By reading the luminescence values (lm) shown on the LCD screen connected with the light meter, the concentration of the target analyte can be derived through comparing to the calibrated values.

6. FUTURE EXPECTATIONS

The biosensor design can be developed overtime to become an applicable product that suits society's needs, and achieve large scale production. To trace slight changes in analyte concentration and improve detection sensitivity, research can be conducted to construct biosensor at single-particle levels. Additional research on constructing the multiple detection sequences helps to establish high-throughput detection of various analytes.

7. CONCLUSION

In summary, an ultrasensitive ECL biosensor is developed for the detection of Aflatoxin using TiO_2 inverse opal as enhanced substrate and CdS quantum dots as a nanomaterial for luminescence. Since TiO_2 inverse opal structure displayed high electrochemical activity, large surface area, and preferable PhC enhancer properties, the ECL emissions

of the modified CdS quantum dots could be significantly enhanced. Because of the acceptable spectrum overlap between CdS quantum dots luminescence wavelength and emission spectrum, highly efficient quenching can be observed which further increases biosensor sensitivity. Therefore, the aptamer-based sandwich immunoassay, antigen-antibody specific binding, and T-Hg^{2+}-T structure, could respectively recognize Aflatoxin B1, Salmonella bacteria, and Mercury Hg^{2+} ions in complex samples efficiently and increase the accuracy of the biosensor. Combining the above strategies, the ultrasensitive ECL biosensor system applied to three major types of food-borne harmful substances is stable, highly sensitive, and time-efficient, which paves an innovative way for the development of new ECL enhanced biosensors and shows great promise in food analysis.

REFERENCES

[1] Carmen J. S, Adam B, Peter B. E et al., The FAO/WHO International Food Safety Authorities Network In Review, 2004-2018: Learning From The Past And Looking To The Future, *Foodborne Pathogen Disease*, (2019) 16 (7), 480-488, doi: 10.1089/fpd.2018.2582.

[2] Lu-xi L, Qin-qin C, Chao-dong Zhang et al., Aflatoxin B1 Causes Oxidative Stress and Apoptosis in Sheep Testes Associated with Disrupting Rumen Microbiota, *Ecotoxicology and Environmental Safety*, 2022 (232), 113225, doi: 10.1016/j.ecoenv.2022.113225.

[3] Mi-ni H, Willie Y, Wei-wei T et al., Genome-Scale Mutational Signatures Of Aflatoxin In Cells, Mice, And Human Tumors, *Genome Research* (2017) 27 (9), 1475-1486, doi:10.1101/gr.220038.116.

[4] Analice K, Martin K, Geert H et al., Local Post-Harvest Practices Associated With Aflatoxin And Fumonisin Contamination Of Maize In Three Agro Ecological Zones Of Tanzania, *Food additives & contaminants Part A, Chemistry, analysis, control, exposure & risk assessment* (2016) 33 (3), 551–559, doi: 10.1080/19440049.2016.1138546.

[5] Anna K, Katarzyna W, Pawel K et al., Aflatoxins: Characteristics And Impact On Human Health, *Postepy higieny i medycyny doswiadczalnej (Online)* (2019) 71 (0), 315–327, doi: 10.5604/01.3001.0010.3816.

[6] Charlie O. P, Yvonne H. L, Mary M et al., Electrochemical Immunochip Sensor For Aflatoxin M_1 Detection, *Analytical Chemistry* (2009) 81 (13), 5291–5298, doi: 10.1021/ac900511e.

[7] Gema CH, Gonzalo MG, Sonia MZ, et al., New Validated Method For The Determination Of Six Opium Alkaloids In Poppy Seed-Containing Bakery Products By High-Performance Liquid Chromatography-Tandem Mass Spectrometry After Magnetic Solid-Phase Extraction, *Journal of Agricultural and Food Chemistry* (2022) 70 (24), 7594–7606, doi: 10.1021/acs.jafc.2c01664.

[8] Su-fang F, Qiang L, Xiao-guang Z et al., Simultaneous Determination Of Aflatoxin B1, B2, G1, And G2in Corn Powder, Edible Oil, Peanut Butter, And Soy Sauce By Liquid Chromatography With Tandem Mass Spectrometry Utilizing Turbulent Flow Chromatographym, *Journal of Separation Science* (2015) 38 (8), 1310–1317, doi: 10.1002/jssc.201401376.

[9] Peterson, J. "Bacterial Pathogenesis." *Nih.gov*, University of Texas Medical Branch at Galveston 2016, www.ncbi.nlm.nih.gov/books/NBK8526/.

[10] Henry D. I., Kominos S., and Marie S, Isolation Of Salmonellae And Shigellae From An Artificial Mixture Of Fecal Bacteria, *Applied microbiology* (1969) 18 (4), 656-9. doi:10.1128/am.18.4.656-659.196

[11] Lazcka O., Del campo F. J., and Muñoz, F. X, Pathogen Detection: A Perspective Of Traditional Methods And Biosensors, *Biosensors & Bioelectronics* (2007) 22 (7), 1205–1217, doi: 10.1016/j.bios.2006.06.036.

[12] World Health Organization, "Mercury And Health", *World Health Organization: WHO*, 31 Mar. 2017.

[13] Chang L, Hai-yang W, Xue-lian H et al., Construction Of An ECL Detection Platform For Sensitive Detection Of Carbaryl Based On An Eu^{3+}-Functionalized Metal-Organic Framework Encapsulated With Nanogold, *Foods* (2022) 11 (10), 1487, doi:10.3390/foods11101487.

[14] Maximillian J, Niclas B, Markus K et al., Electrochemistry Under Confinement, *Chemical Society Reviews* (2022) 51 (7), 2491–2543, doi: 10.1039/D1CS00789K.

[15] Zhen Z, Pei-yao D, Gui-qiang P et al., Utilization And Prospects Of Electrochemiluminescence For Characterization, Sensing, Imaging And Devices, *Materials Chemistry Frontiers* (2019) 3 (11), 2246–2257, doi:10.1039/c9qm00426b.

[16] Chang L, Hai-yang W, Xue-lian H et al., Construction Of An ECL Detection Platform For Sensitive Detection Of Carbaryl Based On An Eu^{3+}-Functionalized Metal-Organic Framework Encapsulated With Nanogold, *Foods* (2022) 11 (10), 1487, doi:10.3390/foods11101487.

[17] Xiao-yan Y, Yi-yan B, Yue-yue H et al., Ultrasensitive Electrochemiluminescence Biosensor Based On Closed Bipolar Electrode For Alkaline Phosphatase Detection In Single Liver Cancer Cell, *Analytical Chemistry* (2021) 93 (3), 1757-1763, doi: 10.1021/acs.analchem.0c04517.
[18] Wen-yue G, Stéphane J, Da-jing Y et al., Electrogenerated Chemiluminescence For Chronopotentiometric Sensors, *Analytical Chemistry* (2019) *91* (7), 4889-4895, doi:10.1021/acs.analchem.9b00787.
[19] Qi-xia S, Giu-zheng Z, and Xiao-li Z, Electrochemiluminescence DNA Sensor Based On Hairpin Structure DNA As Recognition Element And $Ru(Bpy)_3^{2+}$-Doped Silica Nanoparticles As Signal-Producing Compound, *Electroanalysis* (2011) 23, 2693-2698, doi:10.1002/elan.201100331.
[20] Qiu-mei F, Yue-hua G, Jing-juan X et al., Self-Assembled DNA Tetrahedral Scaffolds For The Construction Of Electrochemiluminescence Biosensor With Programmable DNA Cyclic Amplification, *ACS Applied Materials & Interfaces* (2017) *9* (20), 17637-17644, doi:10.1021/acsami.7b04553.
[21] Keijiro O, Yoshiya I, Takayuku E et al., Anionic Polymerization Mechanism Of Acrylonitrile Trimer Anions: Key Branching Point Between Cyclization And Chain Propagation, *The Journal of Physical Chemistry A* (2012) 116 (30), 7937–7942, doi: 10.1021/jp305291r.
[22] Hong Z, Jing L, Jing-juan X et al., Highly Sensitive Electrochemiluminescence Detection Of Single-Nucleotide Polymorphisms Based On Isothermal Cycle-Assisted Triple-Stem Probe With Dual-Nanoparticle Label, *Analytical Chemistry* (2011) 83 (21), 8320-8328, doi: 10.1021/ac2022629.
[23] Nguyen M.M., Gil J., Brown M. et al, Accurate And Sensitive Detection Of *Salmonella* In Foods By Engineered Bacteriophages (2020) 10, 17463, doi: 10.1038/s41598-020-74587-8.
[24] Xin Z, Zhong-jie W, Xu W et al., Band-Edge Effect-Induced Electrochemiluminescence Signal Amplification Based On Inverse Opal Photonic Crystals For Ultrasensitive Detection Of Carcinoembryonic Antigen, *Analytical Chemistry* (2022) 97 (24), 9919–9926, doi: 10.1021/acs.analchem.2c01986.
[25] Shan-shan W, Chuan-ping L, Muhammad S et al., Quasi-Photonic Crystal Light-Scattering Signal Amplification Of SiO_2-Nanomembrane For Ultrasensitive Electrochemiluminescence Detection Of Cardiac Troponin I, *Analytical Chemistry* (2019) 92 (1), 845–852, doi: 10.1021acs.analchem.9b03472.
[26] Xiao-yan W, Kai-di Z, Jin Z et al., Photonic Crystal Of Polystyrene Nanomembrane: Signal Amplification And Low Triggered Potential Electrochemiluminescence For Tetracycline Detection, *Analytical Chemistry* (2021) 93 (5), 2959–2967, doi: 10.1021/acs.analchem.0c04613.
[27] Shan C, Liu-yang G, Mu-huo J et al., Photonic Crystal Enhanced Laser Desorption And Ionization Substrate For Detection Of Stress Biomarkers Under Atmospheric Pressure, *Journal of Materials Chemistry B* (2019) 7 (6), 908–914, doi: 10.1039/C8TB02855A.
[28] Sheng-yuan D and Huang-xian J., Electrogenerated Chemiluminescence Of Nanomaterials For Bioanalysis, *Analyst* (2012) 138 (1), 43–61, doi:10.1039/C2AN36122A.
[29] Xiu-zhen Z and Li-wu Z., Photonic Nanostructures For Solar Energy Conversion, *Energy & Environmental Science* (2016) 9 (8), 2511–2532, doi: 10.1039/c6ee01182a.
[30] Xiu-zhen Z, Su-gang M, Jing C et al., Titanium Dioxide Photonic Crystals With Enhanced Photocatalytic Activity: Matching Photonic Band Gaps Of Tio2 To The Absorption Peaks Of Dyes, *The Journal of Physical Chemistry C* (2013) 117 (41), 21263–21273, doi: 10.1021/jp404519j.
[31] Roman K, Robert M. P, Martin W et al., Bottom-Up Fabrication Of Multilayer Stacks Of 3D Photonic Crystals From Titanium Dioxide, *Applied Materials & Interfaces* (2016) *8* (16), 10466-10476 doi:10.1021/acsami.6b00827.
[32] Yong-fen C and Zeev R., Luminescent CdS Quantum Dots As Selective Ion Probes, *Analytical Chemistry* (2002) 74 (19), 5132–5138, doi: 10.1021/ac0258251.
[33] André A. G. F. B, Rafael M. R, Robson S. R et al., Development And Evaluation Of A Pseudoreference Pt//Ag/Agcl Electrode For Electrochemical Systems, *Industrial & Engineering Chemistry Research* (2012) 51 (14), 5367-5371, doi:10.1021/ie2026025.
[34] Li-na Q, Yoon-hee J, Kelsey A. S et al., Soft-Template-Carbonization Route To Highly Textured Mesoporous Carbon–TiO_2 Inverse Opals For Efficient Photocatalytic And Photoelectrochemical Applications, *Physical Chemistry Chemical Physics* (2014) 16 (19), 9023–9030, doi: 10.1039/c4cp00803k.
[35] I-shuo L, Hsi-hsing L, Chih-tao Chien et al., Enhancing Photoluminescence Quenching And Photoelectric Properties Of CdSe Quantum Dots With Hole Accepting Ligands, *Journal of Materials Chemistry* (2008) 18 (6), 675–682, doi: 10.1039/B715253A.
[36] Qian-qian C, Teng-yue Y, Yu-hang Y et al.,Versatile Photoelectrochemical Biosensing For Hg^{2+} And Aflatoxin B1 Based On Enhanced Photocurrent Of $AginS_2$ Quantum Dot–DNA Nanowires Sensitizing NPc–ZnO Nanopolyhedra, *Analytical Chemistry* (2022) 94 (15), 5814–5822, doi: 10.1021/acs.analchem.1c05250.

[37] Chang-zhi Z, Lu-lu N, Xiao-yu W et al., Small Size Effect And Concentration Response Of Gold Nanoparticles In Electrochemiluminescence Reaction, *Electroanalysis* (2018) 8 (63), doi:10.1002/elan.201900200.
[38] Feng-qin L, Yu-wei L, Ye-ru W et al., Natural Occurrence Of Aflatoxins In Chinese Peanut Butter And Sesame Paste, *Journal of Agricultural and Food Chemistry* (2009) 57 (9), 3519–3524, doi: 10.1021/jf804055n.
[39] Li-wei Y, Zhang S, Xiao-qiang L et al., Detection Signal Amplification Strategies at Nanomaterial-Based Photoelectrochemical Biosensors, *Journal of Materials Chemistry B* (2020) 8 (35), 7880–7893,, doi:10.1039/D0TB01191F.
[40] Ying-qiao H, Guo-dong W, Jun-hong L et al., Cu And Ni Nanoparticles Deposited On ITO Electrode For Nonenzymatic Electrochemical Carbohydrates Sensor Applications, *Electroanalysis* (2016) 29 (4), 965–974, doi: 10.1002/elan.201600606.
[41] Sai-dan X, Feng W, Zhao-yang W et al., A Sensitive Electrogenerated Chemiluminescence Biosensor For Galactosyltransferase Activity Analysis Based On A Graphitic Carbon Nitride Nanosheet Interface And Polystyrene Microsphere-Enhanced Responses, *RSC Advances* (2016) 6 (39), 32804–32810, doi: 10.1039/c6ra05249e.
[42] Ying G, Jing L, Xiao-dong Y et al., Electrochemiluminescence Biosensor Based On PEDOT-PSS- Graphene Functionalized ITO Electrode, *Electroanalysis* (2014) 28, 382-388, doi:10.1002/elan.201300470.
[43] Myung-sung P, Yesol S, Ki-jun K et al., Electrochemical Immunosensor For Human IgE Using Ferrocene Self-Assembled Monolayers Modified ITO Electrode, *Biosensors* (2020) 10 (4), 38, doi:10.3390/bios10040038.
[44] Andrew L. J and James D. P, Recent Developments In Molecular Precursors For Atomic Layer Deposition, *Organometallic Chemistry* (2018) 42, doi: 10.1039/9781788010672-00001.
[45] Nadica D. A, Mirjana I. C, Miroslav D. D et al., Photoluminescence Of Anatase And Rutile TiO_2 Particles, *The Journal of Physical Chemistry* (2006) 110 (50), 25366-25370, doi:10.1021/jp064454f.
[46] Elizabeth R. F, Bryan T. H, Vinod N et al., Scanning Electron Microscopy. *Current Protocols In Microbiology* (2012) 2 (2), doi:10.1002/9780471729259.mc02b02s25.
[47] Zhao Y, and Shuang Z, Photoelectrochemical Sensor, *Reference Module in Biomedical Sciences* (2021), doi:10.1016/b978-0-12-822548-6.00041-8.
[48] Robert D, Peter M, Andreas B et al., Disulfide Bond Formation And Cysteine Exclusion In Gram-Positive Bacteria, *The Journal of biological chemistry* (2010) 285 (5), 3300-3309, doi:10.1074/jbc.M109.081398.
[49] Ranjan S, Whey Proteins In Functional Foods, *Whey Proteins* (2019), 637–663, doi:10.1016/b978-0-12-812124-5.00018-7.
[50] Burr, Holly N., et al, Parasitic Diseases, *Academic Press* (2012), 839–866, doi: 10.1016/b978-0-12-380920-9.00032-8.
[51] J.C. NF, B. H, and J.C. S, Photophysics And Photochemistry Of Aflatoxins B1 And B2, *Photochemical & Photobiological Sciences* (2011) 10 (10), 1701, doi: 10.1039/c1pp05103b.
[52] Bin-yong L, Palanisamy K, Bin Q et al., On-Spot Surface Enhanced Raman Scattering Detection Of Aflatoxin B_1 In Peanut Extracts Using Gold Nanobipyramids Evenly Trapped Into The AAO Nanoholes, *Food Chem* (2020) 307, 125528, doi: 10.1016/j.foodchem.2019.125528.
[53] P. Z, YB. Z, WD. Z et al., Determination of aflatoxins in peanut by high performance liquid chromatography using immunoaffinity column clean-up and on-line electrochemical derivatization, *Se Pu* (2000) 18 (1), 82-84.